

Water Resources Research

RESEARCH ARTICLE

10.1029/2018WR023824

Key Points:

- Experimental/analytical study showing the morphological responses of Gilbert and hyperpycnal deltas to variation of segmented bedrock slopes
- Underlying self-similarities in sediment flux and bed growth rate that come into play for maintaining the self-similar morphologies of delta
- Phase diagrams predicting the trend of morphological shift in Gilbert and hyperpycnal deltas under projected two-slope setting and Q/I ratio

Supporting Information:

- Supporting Information S1

Correspondence to:

F.-C. Wu,
fcwu@ntu.edu.tw

Citation:

Lai, S. Y. J., Chiu, Y.-J., & Wu, F.-C. (2019). Self-similar morphodynamics of Gilbert and hyperpycnal deltas over segmented two-slope bedrock channels. *Water Resources Research*, 55, 3689–3707. <https://doi.org/10.1029/2018WR023824>

Received 2 AUG 2018

Accepted 3 APR 2019

Accepted article online 15 APR 2019

Published online 3 MAY 2019

©2019. American Geophysical Union.
All Rights Reserved.

Self-Similar Morphodynamics of Gilbert and Hyperpycnal Deltas Over Segmented Two-Slope Bedrock Channels

Steven Yueh Jen Lai¹ , Yi-Juei Chiu¹, and Fu-Chun Wu² 

¹Department of Hydraulic and Ocean Engineering, National Cheng Kung University, Tainan, Taiwan, ²Department of Bioenvironmental Systems Engineering, Hydrotech Research Institute, National Taiwan University, Taipei, Taiwan

Abstract Delta progradation over segmented two-slope bedrocks is prevalent in nature, where the bedrock slope upstream or downstream of the slope-break knickpoint is steepened by continued tectonic uplift or subsidence. Understanding the morphodynamics of the most common types of delta in different slope settings is important for interpreting the observed delta progradation into reservoir and predicting delta evolutions under future tectonic/climate scenarios or anthropogenic interventions. Here, we present an experimental and analytical study demonstrating the morphological responses of Gilbert-type and hyperpycnal deltas to variations of bedrock slopes. Steepening the upstream slope accelerates shoreline migration; steepening the downstream slope decelerates shoreline migration. In either case, the subaqueous volume is enhanced yet the subaerial volume is reduced. Both types of delta exhibit self-similar morphologies when evolving over segmented bedrocks. Hyperpycnal deltas, through enhanced sediment fluxes driven by dense underflows, develop larger subaqueous volumes. We further demonstrate the underlying self-similarities in sediment flux and bed growth rate that come into play for attaining the self-similar morphologies. The combined effect of flowrate (Q) and sediment supply rate (I) may be characterized by a dimensionless Q/I ratio. Increasing Q/I advances the entire delta. For Gilbert deltas, shoreline migration accelerates with Q/I . For hyperpycnal deltas, shoreline migration exhibits a “first-accelerate-then-decelerate” trend with Q/I in a limited range of slope combinations close to the single-slope setting, indicating that the effect of Q/I emerges only when the two-slope effect is weak or absent. Away from this near-single-slope range, the two-slope effect becomes dominant, thus suppressing the effect of Q/I .

1. Introduction

A delta is a depositional feature that develops where a sediment-laden river (alluvial or bedrock) enters a basin, such as lake or reservoir, and loses its sediment transport capacity. This study focuses on delta evolutions in bedrock rivers. The longitudinal profile of a delta consists of a subaerial region above base level and a subaqueous region below base level, separated by a shoreline (Figure 1). Supplied by the sediment yields of seasonal high-flow events (Amos et al., 2004; Uchida et al., 2018), the supply-limited sediment transport drapes deltaic deposits over the bedrock channel both upstream and downstream of the advancing shoreline (Figures 2a and 2b). Upstream, aggradation of topset drives headward migration of bedrock-alluvial transition. Downstream, sediments transported to shoreline allow progradation of foreset into the basin (Muto, 2001). In cases where the wave and tidal forcings are negligible, along the foreset sediment transport is driven by either (1) gravitational avalanching (Figure 2a) if the entering flow is lighter than the receiving basin (hypopycnal) or neutrally buoyant (homopycnal) or (2) plunging underflow (Figure 2b) if the turbid inflow is heavier than the ambient (hyperpycnal) (Lai & Capart, 2007).

For homopycnal or hypopycnal flows, a sudden reduction in tractive force is experienced at the shoreline (Lai & Capart, 2007), giving rise to a steeply sloping foreset governed by angle-of-repose avalanching of coarser sediment (Figure 2a), rendering the finer suspended fractions to settle out further downstream as a bottomset. Such deltas, along with their topset-foreset-bottomset structure, are well known as Gilbert-type deltas (Gilbert, 1890). In this study, we focus on deposition of relatively coarse sediment along the topset and foreset, neglecting bed elevation change due to finer suspended sediment settling out as bottomset. For hyperpycnal flows, the denser turbid inflow will plunge down the bottom of the basin and continue its path in the form of density current (Figure 2b). Since density stratification suppresses turbulent entrainment, such density current tends to keep its identity instead of fully mixing with the overlying ambient,

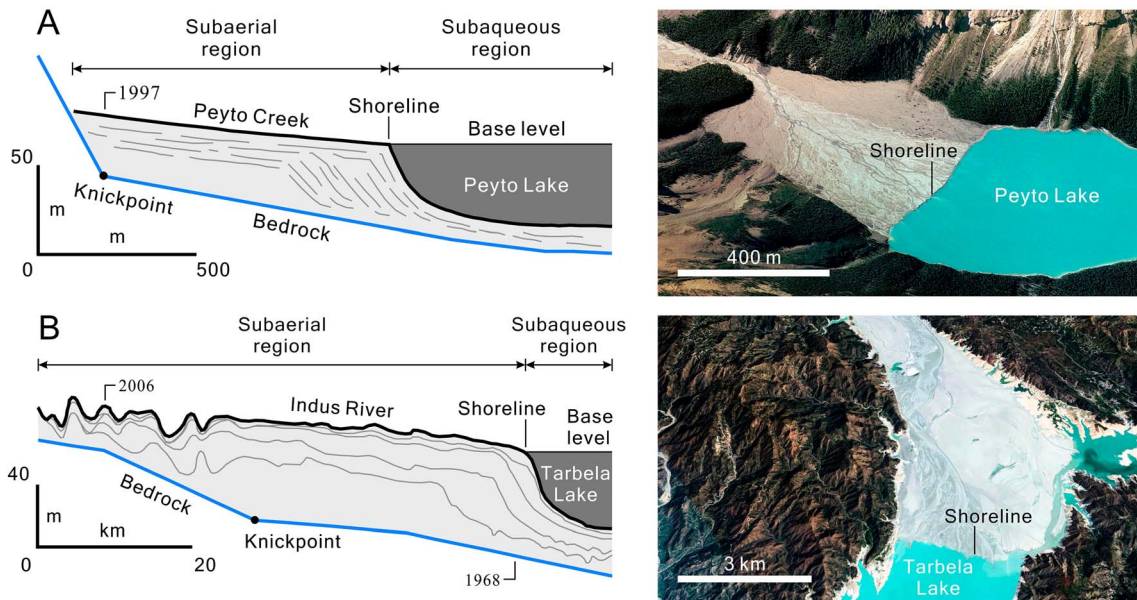


Figure 1. (a) Peyto delta (Banff National Park, Canada): longitudinal profile of Gilbert-type delta (based on data from Smith & Jo1, 1997, and Chikita et al., 1996), and Google Earth image of topset and shoreline; (b) Tarbela delta (upper Indus River, Pakistan): longitudinal profile of hyperpycnal delta (modified from Ahmed & Sanchez, 2011), and Google Earth image of topset and shoreline.

allowing the turbidity current to travel over a longer distance. The along-bed deposits contribute to foreset progradation. Thus, hyperpycnal deltas are characterized by longer and milder foresets than their Gilbert-type counterparts (Kostic et al., 2002).

The bedrock channels over which deltas develop may have uniform or gradually varying slopes or exhibit segmented bottom profiles marked by distinct slope-break knickpoints (Figure 1). Bedrock channels can accommodate changes in tectonic forcing by adjustment of bed slope and formation of knickpoint

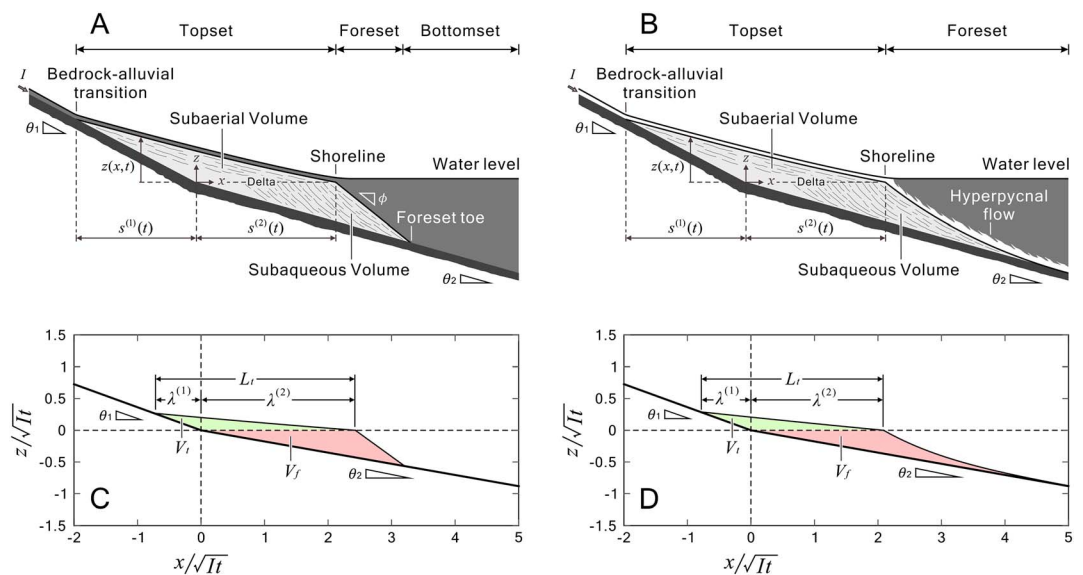


Figure 2. Definition sketches of Gilbert delta (a and c) and hyperpycnal delta (b and d): (a, b) longitudinal profile of delta evolving over segmented two-slope bedrock; (c, d) scaled (normalized) dimensions of self-similar delta profile over segmented two-slope bedrock. See text for notations.

(Ahmed et al., 2018; Kirby & Whipple, 2012; Whipple et al., 2013). Two field examples are given here (Figure 1). The Peyto Creek delta (Banff National Park, Canada) is a small Gilbert-type delta developing over the bedrock of a glacially deepened valley (Smith & Jo1, 1997). Upstream of the knickpoint the bedrock dips at 20° , as opposed to the mild bedrock downstream of the knickpoint. The delta is $\sim 1,000$ m long and 750 m wide at the lake, forming a gravel valley-fill confined by steep valley sides (Figure 1a). Ground-penetrating radar facies reveal the topset beds having a slope of 1.1° , foresets having a slope of 25° , and fine-grained bottomset beds. In contrast, the reservoir-infilling Tarbela delta (upper Indus River, Pakistan) is a hyperpycnal delta developing over a bedrock with steeper upstream basement (Ahmed & Sanchez, 2011). The delta is mainly composed of sand and silt (Figure 1b), transported in the form of turbidity current by summer runoff from snow and glacier melt. Progradation of foreset was faster than expected (World Commission on Dams, 2000). In 2006 the foreset front reached a point 11 km away from the dam, threatening the low-level outlets and power plant that could be blocked by liquefied sediment induced by earthquakes common in this region (Ahmed & Sanchez, 2011).

Despite being prevalent in nature, progradation of delta over segmented bedrocks has remained largely unexplored until recently. Lai, Hsiao, and Wu (2017) presented an experimental and analytical study investigating the longitudinal profiles of Gilbert deltas evolving over segmented bedrocks with unequal upstream and downstream basement slopes. They demonstrated that the scaled profiles of an evolving delta collapse to a single profile, allowing the analytical self-similar profiles to be used for studying the morphological responses to variations of basement slopes. Steepening the upstream or downstream slope increases the subaqueous delta volume yet reduces the subaerial volume. These findings may carry important implications for delta progradation into reservoir over segmented bedrocks where the upstream or downstream slope is steepened by tectonic uplift or subsidence.

As mentioned above, Gilbert and hyperpycnal deltas develop through different mechanisms, and exhibit different morphologies particularly over the foreset. It is, however, still unclear as to whether the observed morphological responses of Gilbert deltas to variations of bedrock slopes apply also to hyperpycnal deltas. For example, it is unclear why progradation of hyperpycnal delta into the Tarbela Reservoir was faster than expected despite that the average sediment inflow was lower than predicted (World Commission on Dams, 2000). The following research questions remain to be asked. (1) Would a hyperpycnal delta also exhibit self-similar morphologies when evolving over segmented bedrocks? (2) Would a delta need to exhibit self-similar sediment flux and bed growth rate in order to maintain the self-similar morphology? (3) Under identical slope, flow and sediment conditions, what are the morphological responses of hyperpycnal deltas relative to those of Gilbert deltas? (4) What is the combined effect of flow and sediment supply on progradation of delta in different slope settings? (5) Would this combined effect be similar in Gilbert and hyperpycnal deltas? Answering these questions would provide useful information for interpreting progradation of delta into a basin under different tectonic and climatic forcings and anthropic disturbances. To this aim, we perform an experimental and analytical study to investigate the morphodynamics of Gilbert and hyperpycnal deltas evolving over segmented bedrock channels.

This paper is structured as follows. In section 2, we summarize the analytical and experimental methods used. In section 3, the delta morphologies under different slope settings, flow, and sediment supply conditions are compared and the underlying self-similarities are discussed. In section 4, two types of phase diagram for morphological features of Gilbert and hyperpycnal deltas are presented and their practical implications are discussed, followed by the conclusions reported in section 5.

2. Methods

2.1. Analytical Approaches

The analytical approaches used in this study include: Part 1: morphodynamic model of Gilbert delta; Part 2: morphodynamic model of hyperpycnal delta; Part 3: along-delta sediment flux and bed growth rate. The full derivations of these analytical approaches are provided in the supporting information. For Part 1, the geomorphic actions of fluvial flow over the topset are modeled as a single-diffusion process while the bedrock-alluvial transition and shoreline are treated as two moving boundaries (Figure 2a). This has been presented previously (Lai, Hsiao, & Wu, 2017), thus is only briefly summarized (Text S1). For Part 2, the geomorphic actions of turbid streamflow over the topset and dense underflow over the foreset are modeled as a

two-diffusion process with two moving boundaries (Figure 2b). This is one contribution of this work. We extend the analytical framework of Lai and Capart (2009) by incorporating the two-slope setting (Text S1). A similarity solution for the evolving delta profile $z(x,t)$ is obtained following a scaling approach used in the prior works (e.g., Capart et al., 2007; Lai & Capart, 2009; Lai, Hsiao, & Wu, 2017; Lorenzo-Trueba et al., 2009; Voller et al., 2004), which may be expressed in a general form:

$$z(x,t)/\sqrt{It} = f\left(x/\sqrt{It}\right) \quad (1)$$

where I is the volumetric sediment supply rate per unit width (Figures 2a and 2b); x/\sqrt{It} ($=\bar{x}$) and z/\sqrt{It} ($=\bar{z}$) are, respectively, the scaled (normalized) horizontal coordinate and bed surface elevation (Figures 2c and 2d). Equation (1) indicates that the length and height of the delta evolve according to the self-similar profile governed by the dimensionless shape function $f(\bar{x})$ and time-varying length scale \sqrt{It} . Equation (1) is used to examine the self-similar profiles of the evolving delta observed in each experiment. The scaled positions of bedrock-alluvial transition and shoreline, $s^{(1)}(t)/\sqrt{It} = \lambda^{(1)}$ and $s^{(2)}(t)/\sqrt{It} = \lambda^{(2)}$, and scaled profile of the evolving delta, $z(x,t)/\sqrt{It} = f(\bar{x})$, are time-invariant under constant boundary conditions (including I and base level). It follows that the migration rates of bedrock-alluvial transition and shoreline, $ds^{(1)}/dt$ and $ds^{(2)}/dt$, and the local bed growth rate $\partial z/\partial t$ are all varying as a function of $1/\sqrt{t}$, implying that the growth of delta would slow down with time.

In our analytical model and flume experiments (Figures 2 and 3) the base level is fixed and aligns with the origin (slope-break knickpoint). Such boundary condition allows us to derive an analytical solution using the similarity structure and to reveal the self-similar morphology of an evolving delta. Without such simplification, the geometric complexities would demand a numerical solution in place of a transparent, analytical solution. Alternatively, the base level could be varied in proportion to the time-varying length scale \sqrt{It} , and a much complicated analytical solution can be derived following a previous case study that considered delta progradation into a breached lake (Capart et al., 2007). Both of the above options are, however, out of the scope of this study, which is to demonstrate the self-similar morphologies, sediment fluxes, and bed growth rates of Gilbert and hyperpynal deltas evolving over segmented bedrocks. The analytical model based on ideal assumptions may not be directly applicable to many real-world problems. However, it provides a valuable tool for gaining physical insights and shedding new light on key morphological processes. Moreover, the results associated with constant base level may well approximate those observed in such natural settings where the base level change is slow in time or small in amplitude (Chavarrias et al., 2018).

Last, as a continuous profile of sediment flux along the delta is hard to measure experimentally, using the observed or analytical delta profile to reconstruct the along-delta sediment flux can be a useful approach. For Part 3, the following formula (see Text S2 for derivation) is used to reconstruct the normalized profile of sediment flux $\bar{j} = j(s,t)/I$ at location s using each delta profile $z(x,t)$:

$$\bar{j} = 1 + \frac{[z(s,t) - z_0(s)]s}{2I} - \frac{1}{It} \int_{-\infty}^s [z(x,t) - z_0(x)] dx \quad (2)$$

where z_0 is the elevation of bedrock; $z - z_0$ is the thickness of bed sediment. The normalized differential sediment flux $\partial \bar{j}/\partial \bar{x}$ is then used to evaluate the normalized bed growth rate $\overline{\partial z/\partial t}$ (Text S2), as expressed by

$$\overline{\partial z/\partial t} = -\partial \bar{j}/\partial \bar{x} \quad (3)$$

where $\overline{\partial z/\partial t} = (\partial z/\partial t)/\sqrt{I/t}$. The along-delta profiles of sediment flux and bed growth rate are used to examine whether these underlying self-similarities do exist in evolving deltas.

2.2. Experiments

Flume experiments are performed to observe the evolution of delta morphology over segmented bedrock channels having different combinations of upstream and downstream slope angles (θ_1, θ_2). Figure 3 is the experimental setup, which consists of a water tank 1.8 m (length) by 20 cm (width) by 65 cm (height) and an internal sediment flume 1 cm in width. The sediment flume is composed of acrylic bedrock floor and sidewalls. The bedrock floor is replaceable for different (θ_1, θ_2). A thin layer of sediment is glued on the bedrock floor to create suitable roughness. An overflow weir is used to maintain a constant water level. A

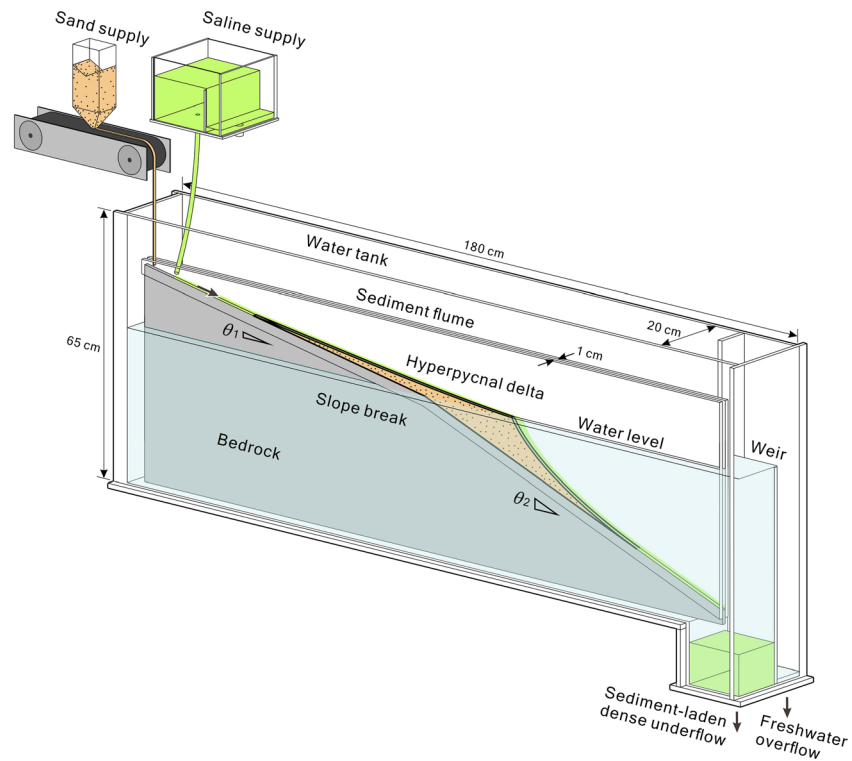


Figure 3. Experimental setup for hyperpycnal delta evolving over segmented two-slope bedrock with different upstream and downstream basement slopes.

conveyor-belt sand supplier and a constant-head saline supplier are installed above the tank; a drain system for the sediment-laden dense underflow and freshwater overflow is installed at the downstream end. For Gilbert delta experiments, saline is replaced with freshwater, and the drain for the sediment-laden underflow is not used.

Before each run, the sediment flume was fixed on an aluminum support and partly immersed. To be consistent with the base-level setting of the analytical model, the water level was set to align with the slope break of the bedrock. Steady unit discharge Q and sediment influx I were supplied. A saturated brine with density $\rho_{in} = 1,200 \text{ kg/m}^3$ was used as a surrogate for the mud-rich turbidity current (e.g., Foreman et al., 2015; Lai & Capart, 2007; Lai et al., 2016; Lai, Hung, et al., 2017; Métivier et al., 2005). Ottawa standard sand (median size $d_{50} = 0.17 \text{ mm}$, density $\rho_s = 2670 \text{ kg/m}^3$, and in-water angle of repose $\phi = 36^\circ$) was used, which provided coarse-grained material for delta deposits. Fluorescent dye was added to saline for visualization of underflows; coal ash was sprinkled from the upstream at constant intervals to visualize the stratigraphy of delta deposits (Figures 4a–4c and 5a–5c). Time-lapse photography was used to monitor delta evolutions, with images acquired every 5 s using a digital single-lens reflex camera. Each run lasted for 1,700 s before the length of delta exceeded the extent of the flume. Delta profiles were extracted by digitizing the images and converting pixel to physical coordinates using a calibrated linear transform.

Two series of experiments, a total of 18 runs were performed (Table 1), Series H and G stand for hyperpycnal and Gilbert delta experiments, respectively. Three slope settings were used: (1) steeper upstream slope, $(\theta_1, \theta_2) = (20^\circ, 10^\circ)$; (2) equal upstream and downstream slopes (i.e., single-slope setting), $(\theta_1, \theta_2) = (10^\circ, 10^\circ)$; (3) steeper downstream slope, $(\theta_1, \theta_2) = (10^\circ, 15^\circ)$. For each slope setting, we performed a set of three runs with a high Q/I ratio ($=28.5 \pm 0.8$), a medium Q/I ratio ($=18.3 \pm 0.2$), and a low Q/I ratio ($=9.6 \pm 0.4$). These experiments were designed to investigate the effects of (θ_1, θ_2) and Q/I ratio on hyperpycnal and Gilbert deltas. The slope angles used are consistent with the reported range ($1^\circ - 38^\circ$) for the bedrock rivers in mountain areas (Montgomery & Buffington, 1997) and bedrock channels in coastal badlands (Howard & Kerby, 1983).

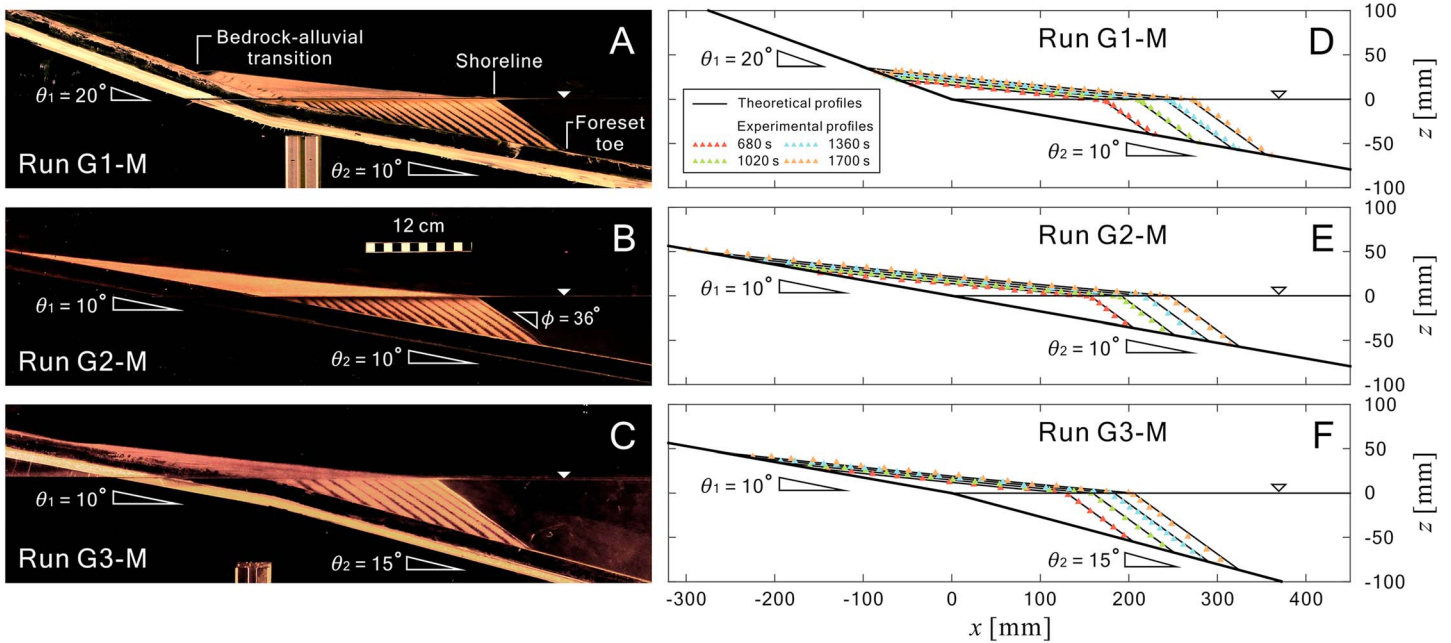


Figure 4. Gilbert deltas (Runs G1-M, G2-M, and G3-M) in different slope settings under constant Q/I ratio ($=18.3 \pm 0.2$): (a–c) photographs showing delta profiles at the end of runs ($t = 1,700$ s); (d–f) theoretical and experimental profiles of evolving deltas.

It should be noted that the Q/I ratios used in our experiments (about 10, 20, and 30) are aimed to create supply-limited conditions; that is, the sediment supply rate I is less than the transport capacity associated with the flowrate Q , so that sediment will not deposit before reaching the aggrading delta. These Q/I ratios are smaller than typical values of Q/I ($\gg 100$) observed in many supply-limited rivers (Carraro et al., 2018; Lanzoni et al., 2006). The smaller values of Q/I would only accelerate the buildup of delta without affecting

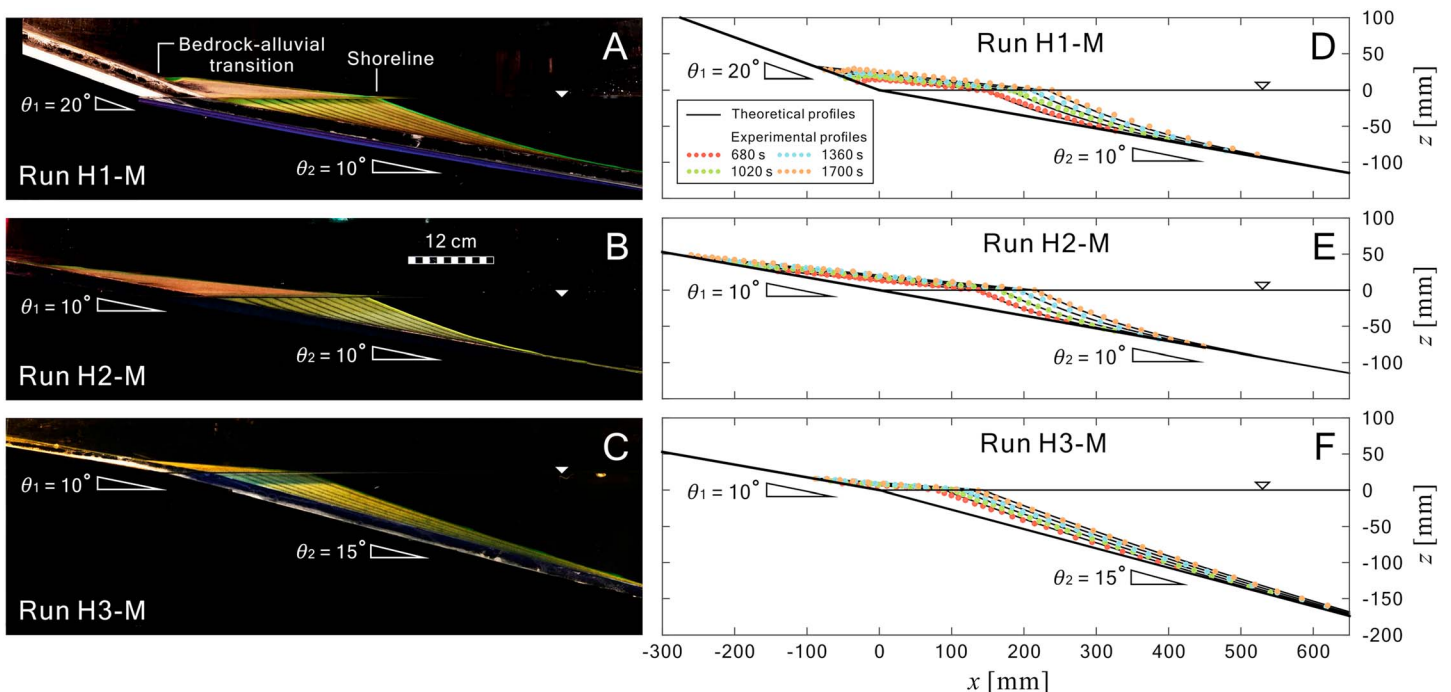


Figure 5. Hyperpycnal deltas (Runs H1-M, H2-M, and H3-M) in different slope settings under constant Q/I ratio ($=18.3 \pm 0.2$): (a–c) photographs showing delta profiles at the end of runs ($t = 1,700$ s); (d–f) theoretical and experimental profiles of evolving deltas.

Table 1
Summary of Experimental Conditions (18 Runs)

Type of delta	Run	θ_1 (deg)	θ_2 (deg)	Q (mm ² /s)	I (mm ² /s)	Q/I (-)	Fr_1 (-)	Fr_2 (-)
Hyperpycnal	H1-H	20	10	272.7	9.88	27.6	2.09	0.97
	H1-M	20	10	141.6	7.75	18.3	1.24	0.65
	H1-L	20	10	70.7	7.40	9.6	0.71	0.62
	H2-H	10	10	217.8	7.76	28.1	1.67	0.78
	H2-M	10	10	140.0	7.71	18.2	1.23	0.64
	H2-L	10	10	71.1	7.14	10.0	0.72	0.62
	H3-H	10	15	266.1	9.13	29.1	2.04	0.95
	H3-M	10	15	147.8	8.01	18.5	1.29	0.67
	H3-L	10	15	73.0	7.81	9.3	0.74	0.64
Gilbert	G1-H ^a	20	10	275.0	9.57	28.7	2.11	
	G1-M ^a	20	10	140.0	7.64	18.3	1.23	
	G1-L ^a	20	10	75.8	7.94	9.5	0.76	
	G2-H ^a	10	10	275.0	9.57	28.7	2.11	
	G2-M ^a	10	10	138.8	7.49	18.5	1.21	
	G2-L ^a	10	10	76.0	7.91	9.6	0.77	
	G3-H	10	15	219.0	7.68	28.5	1.68	
	G3-M	10	15	141.7	7.85	18.1	1.24	
	G3-L	10	15	72.0	7.45	9.7	0.73	

Note. Fr_1 and Fr_2 are Froude numbers over the topset and foreset, respectively.

^aData from Lai, Hsiao, and Wu (2017).

the underlying physical processes because, even if the flows are transcritical (see Table 1 for Froude numbers over topset and foreset), deltas are long diffusion waves of bedform so that propagation of hydrodynamic fronts is too fast to be affected by sediment transport (Lanzoni et al., 2006; Sun et al., 2002).

3. Results and Discussion

In this section we investigate the results of Gilbert and hyperpycnal delta experiments regarding: (1) the morphological response to variation of upstream or downstream slope; (2) the self-similarities in evolving delta morphology, sediment flux and bed growth rate; and (3) the morphological response to variation of Q/I . The experimental observations are also compared with the theoretical results.

3.1. Two-Slope Effects on Gilbert and Hyperpycnal Deltas

Figures 4a–4c and 5a–5c are photos showing the profiles of Gilbert and hyperpycnal deltas at the end of runs in various slope settings (under constant Q/I ratios). Gilbert deltas are characterized by a sloping foreset held at the angle of repose, with a distinct toe observed at the front. For hyperpycnal deltas, no distinct toes were observed since the dense underflows transported sediment over longer distances. The deltaic responses to steepening of upstream and downstream segments are asymmetric (Lai, Hsiao, & Wu, 2017). Take the single-slope experiment (Run G2-M, H2-M) as the reference case, steepening the upstream slope would accelerate shoreline migration (Run G1-M, H1-M), whereas steepening the downstream slope would decelerate shoreline migration (Run G3-M, H3-M). In either case, the subaqueous delta volume is increased in compensation for the reduced topset dimensions.

The observed evolving profiles of Gilbert and hyperpycnal deltas are in good agreement with the theoretical profiles (Figures 4d–4f and 5d–5f), including the aggrading topsets and prograding foresets. In particular, the significant difference between the foresets of Gilbert and hyperpycnal deltas is well captured by the theory. The observed effects of upstream and downstream basement slopes on the migration rates of bedrock-alluvial transition and shoreline are captured as well. Also observed are the decreasing trends of shoreline migration rate and bed growth rate as a function of $1/\sqrt{I}$, in agreement with the theory (see section 2). Figure 6 shows the experimental and theoretical trajectories of the two moving boundaries. Compared to the single-slope reference case (Figure 6b), steepening the upstream slope (Figure 6a) causes the shoreline to migrate farther downstream while restricts the headward migration of bedrock-alluvial transition. Steepening the downstream slope (Figure 6c), however, suppresses both boundary migrations.

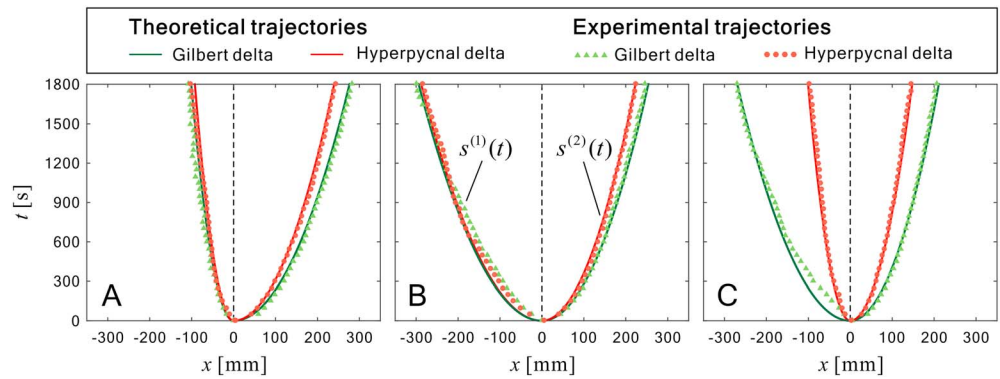


Figure 6. Theoretical and experimental trajectories of two moving boundaries: (a) Runs G1-M and H1-M ($\theta_1 = 20^\circ$, $\theta_2 = 10^\circ$), (b) Runs G2-M and H2-M ($\theta_1 = \theta_2 = 10^\circ$), and (c) Runs G3-M and H3-M ($\theta_1 = 10^\circ$, $\theta_2 = 15^\circ$; $s^{(1)}(t)$ = evolving position of bedrock-alluvial transition, and $s^{(2)}(t)$ = evolving position of shoreline).

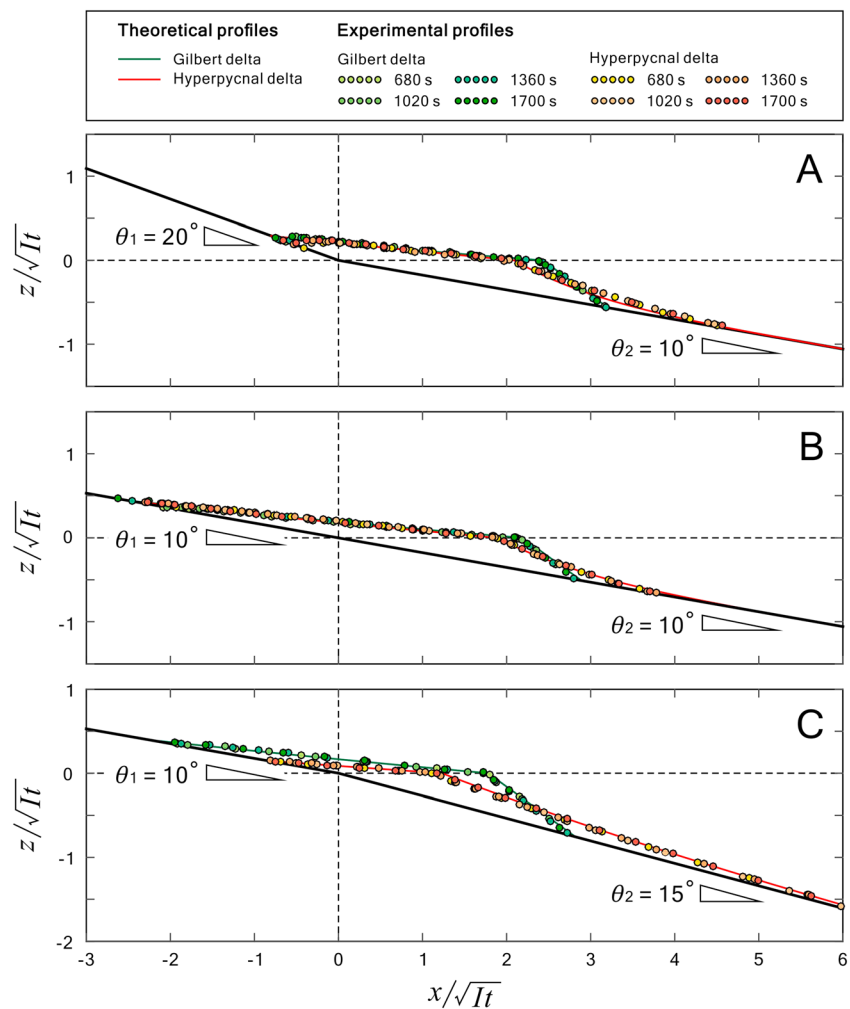


Figure 7. Scaled profiles of evolving Gilbert and hyperpycnal deltas showing the morphological self-similarity in different slope settings under constant Q/I ratio ($=18.3 \pm 0.2$): (a) Runs G1-M and H1-M; (b) Runs G2-M and H2-M; (c) Runs G3-M and H3-M.

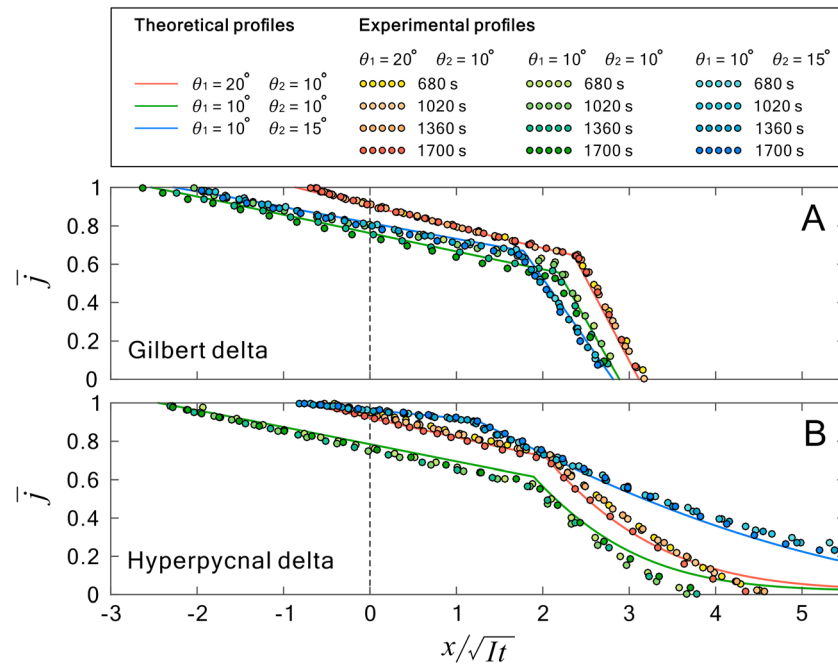


Figure 8. Scaled profiles of \bar{j} ($= j/I$) versus x/\sqrt{It} ($= \bar{x}$) demonstrating the self-similarity of sediment flux in different slope settings under constant Q/I ratio ($=18.3 \pm 0.2$): (a) Gilbert deltas (Runs G1-M, G2-M, and G3-M); (b) hyperpycnal deltas (Runs H1-M, H2-M, and H3-M).

In either case, the decrease in topset length $s^{(2)}(t) - s^{(1)}(t)$ (see Figure 2 for notations) is particularly evident for hyperpycnal deltas.

3.2. Self-Similar Morphology, Sediment Flux, and Bed Growth Rate

To examine whether an evolving delta would exhibit self-similar morphologies, in Figure 7 we show the scaled profiles of Gilbert and hyperpycnal deltas in different slope settings (under constant Q/I). For each case considered, the scaled profiles of an evolving delta (from t_1 to t_4) collapse to a single theoretical profile, indicating that a morphological self-similarity is established consistently. Such self-similar profiles allow for a comparison of the results associated with different types of delta, different slope settings, or different Q/I ratios. For example, compared to the single-slope reference case (Figure 7b), a steeper upstream slope suppresses the headward expansion of topset in both types of delta (Figure 7a). A steeper downstream slope exerts a particularly significant effect on hyperpycnal deltas, enhancing the development of foreset at the price of reduced topset dimensions (Figure 7c). Due to the enhanced development of foreset in hyperpycnal deltas, shoreline migrations are suppressed compared to the results observed in Gilbert deltas.

The along-delta sediment fluxes \bar{j} are evaluated with the integral formula, equation (2), using the experimental and theoretical delta profiles. The resulting profiles of \bar{j} versus \bar{x} for Gilbert and hyperpycnal deltas are shown in Figure 8. Similar to Figure 7, for each case the scaled profiles of sediment flux collapse to a single theoretical profile, indicating that a self-similarity in sediment transport is established consistently. At the shoreline, a break in sediment flux is present due to the transition from topset to foreset. Over the topset, both Gilbert and hyperpycnal deltas exhibit mild declining trends. Over the foreset, however, declining trends become steeper, where fairly different profiles of sediment flux are observed in different types of delta. Gilbert deltas have sediment fluxes declining linearly to zero, primarily attributed to the linear profiles of foreset. Hyperpycnal deltas, in contrast, exhibit concave profiles of sediment flux declining more slowly and asymptotically toward the distal pinch-out, mainly due to the elongated, concave profiles of foreset. At the distal pinch-out, the discrepancy between the experimental and theoretical profiles may arise from the digitization errors or mathematics itself. The digitization errors were especially significant for very thin foreset fronts, as in Runs H1-M and H2-M (Figures 5d and 5e). These errors diminished for runs with thicker foreset fronts, as in Run H3-M (Figure 5f).

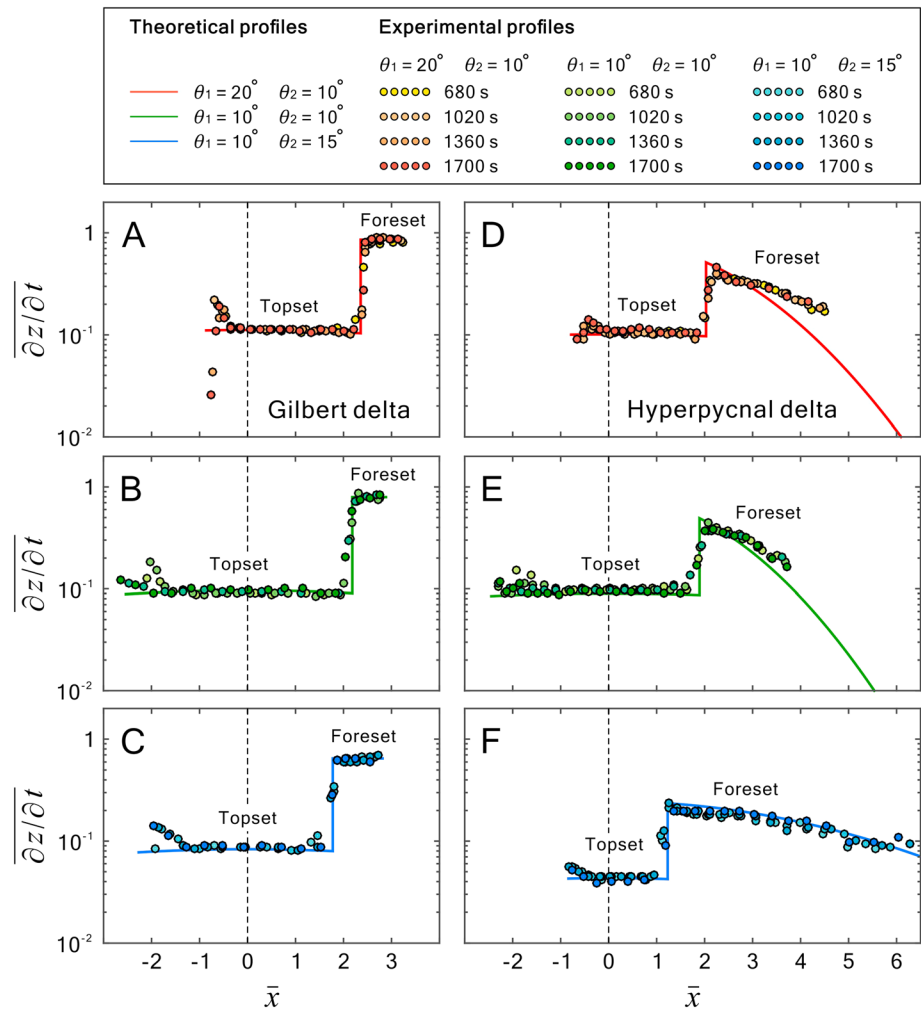


Figure 9. Scaled profiles of $\overline{\partial z/\partial t}$ versus x/\sqrt{It} ($=\bar{x}$) demonstrating the self-similarity of bed growth rate in different slope settings under constant Q/I ratio ($=18.3 \pm 0.2$): (a–c) Gilbert deltas (Runs G1–M, G2–M, and G3–M); (d–f) hyperpycnal deltas (Runs H1–M, H2–M, and H3–M).

We then use the profiles of \bar{z} versus \bar{x} and equation (3) to evaluate the scaled bed growth rates. The resulting profiles of $\overline{\partial z/\partial t}$ versus \bar{x} for different types of delta are shown in Figure 9. Similar to Figures 7 and 8, for each case the experimental profiles of $\overline{\partial z/\partial t}$ versus \bar{x} collapse to a single theoretical profile, indicating that a consistent self-similarity in bed growth rate is established. In each subplot, the bed growth rate over topset is nearly constant, leading to a quasi-parallel aggradation of topset (as in Figures 4d–4f and 5d–5f). Over the foreset, constant growth rates of Gilbert deltas are evidenced by parallel foreset progradation (Figures 4d–4f). By contrast, the growth rates of foreset in hyperpycnal deltas decline rapidly toward the foreset front, giving rise to a vanishingly small thicknesses toward the distal pinch-out (Figures 5d–5f). For either type of delta, however, across the shoreline a sudden rise in bed growth rate indicates that the primary area of deposition and delta development is over the foreset, particularly in the nearshore zone. Compared to the single-slope case of hyperpycnal delta (Figure 9e), a steeper downstream slope promotes a more uniform bed growth rate over the foreset (Figure 9f), achieved at the cost of a much reduced growth rate over the topset, which in turn leads to a larger foreset, a smaller topset, and a slower shoreline migration (Figure 7c).

To facilitate a more straightforward comparison, the theoretical profiles given in Figures 7–9 are aligned on the shorelines at a shifted origin $\bar{x}_s = 0$ (Figure 10), where $\bar{x}_s < 0$ is for topset, $\bar{x}_s > 0$ is for foreset. This way the responses of sediment flux and bed growth rate to slope variation become apparent. Compared to the single-slope case, a steeper upstream slope enhances the topset elevation growth rather than headward expansion (Figures 10c and 10f) to increase the gradient of sediment flux (Figures 10b and 10e). By contrast, a steeper

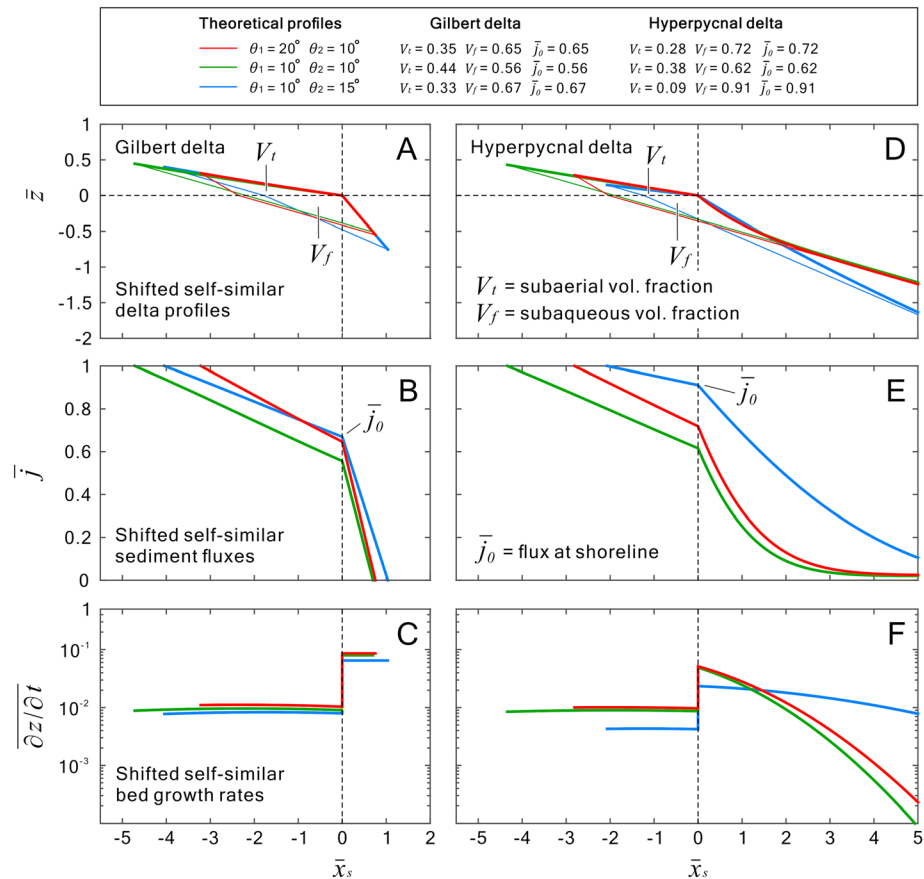


Figure 10. Self-similar profiles (from Figures 7–9) aligned on their shorelines at shifted origin $\bar{x}_s = 0$: (a) and (d) delta profiles, (b) and (e) sediment fluxes, (c) and (f) bed growth rates established in different slope settings under constant Q/I ratio ($=18.3 \pm 0.2$). Left column: Gilbert deltas (Runs G1-M, G2-M, and G3-M); right column: hyperpycnal deltas (Runs H1-M, H2-M, and H3-M).

downstream slope restricts the topset elevation growth and headward expansion such that the gradient of sediment flux is reduced. These responses in the gradient of transport over the topset are attributed to the shoreline migration rate, shown in Figure 7, where a steeper upstream slope accelerates shoreline migration whereas a steeper downstream slope decelerates shoreline migration. Similar responses are also observed in the foresets of Gilbert deltas and nearshore foresets of hyperpycnal deltas. Here, we demonstrate the underlying self-similarities in sediment flux and bed growth rate that come into play for attaining the self-similar morphology of an evolving delta, an argument that was raised yet untested in a previous numerical study of sand-ripple morphodynamics (Zgheib et al., 2018).

In response to steepening of upstream or downstream slope, the topset is shortened while the foreset is lengthened consistently (Figures 10a and 10d). The resulting subaerial and subaqueous volumes V_t and V_f are, respectively, smaller and greater than the corresponding values in the single slope. The flux \bar{j}_0 at the shoreline is equal to the subaqueous volume V_f (Figures 10b and 10e), since \bar{j}_0 is the fraction of sediment supply delivered to the foreset. The fluxes in the two-slope settings are invariably greater than those in the single slope. Among all cases with steeper downstream slope, the foreset of hyperpycnal delta exhibits the greatest sediment flux, which results in a more uniform bed growth rate over the foreset (Figure 10f).

3.3. Effects of Q/I Ratio on Gilbert and Hyperpycnal Deltas

The effects of Q/I ratio on different types of delta are shown in Figure 11, where each subplot includes three delta profiles associated with different Q/I ratios. For Gilbert deltas, increasing Q/I advances the entire delta, leading to a smaller topset length L_t and a greater subaqueous volume V_f (Lai, Hsiao, & Wu, 2017). These

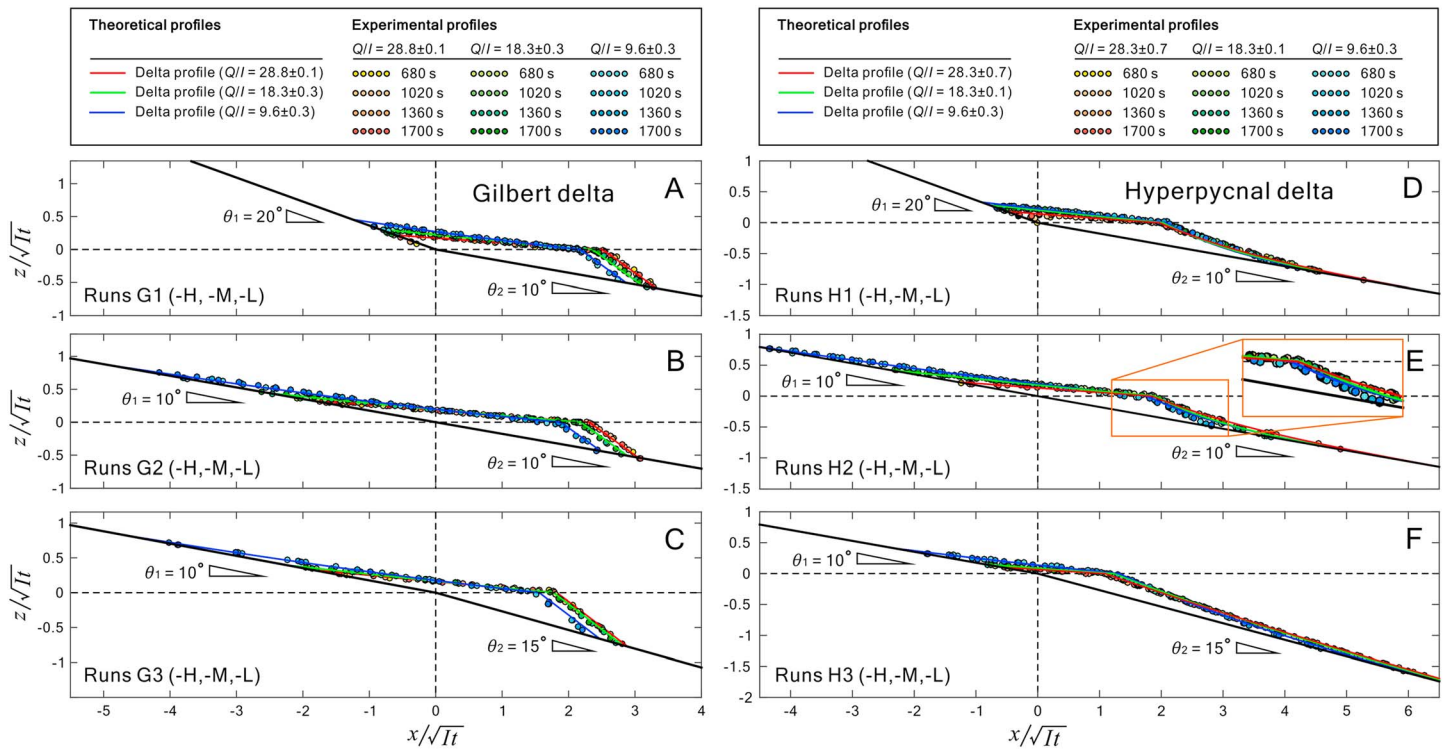


Figure 11. Self-similar profiles of delta showing the effects of Q/I ratio on Gilbert deltas (left column) and hyperpycnal deltas (right column) in different slope settings: (a and d) $\theta_1 = 20^\circ$, $\theta_2 = 10^\circ$; (b and e) $\theta_1 = \theta_2 = 10^\circ$; (c and f) $\theta_1 = 10^\circ$, $\theta_2 = 15^\circ$.

effects are clearly demonstrated in Figures 12a–12c, where the increase of Q/I invariably accelerates the migration of shoreline $\lambda^{(2)}$, reduces the topset length L_t , and increases the subaqueous volume V_f . For hyperpycnal deltas, the effects of Q/I on L_t and V_f (Figures 12e and 12f) are similar to those observed in Gilbert deltas (Figures 12b and 12c), while the effect on shoreline migration (Figure 12d) is different from those observed in Gilbert deltas (Figure 12a). In the two-slope settings, shoreline migration decelerates monotonically with increasing Q/I (Figures 11d and 11f), whereas in the single-slope setting shoreline migration exhibits a subtle “first-accelerate-then-decelerate” trend with increasing Q/I (Figure 11e). Although very subtle, such trend does exist outside of noise and is only observed in hyperpycnal deltas, present primarily in the single-slope settings but also in the near-single-slope settings (see section 4.1 for further discussion).

To further compare the morphological responses of Gilbert and hyperpycnal deltas, we show in Figures 12g–12i the agreement plots of shoreline $\lambda^{(2)}$, topset length L_t , and subaqueous volume V_f . The data points in Figures 12g and 12h are all on the lower-right side of the 1:1 line of perfect agreement, while those in Figure 12i are all on the upper-left side. Overall, Gilbert deltas exhibit faster shoreline migrations and longer topsets, while hyperpycnal deltas exhibit greater subaqueous volumes. These results indicate that, through the enhanced sediment flux driven by dense underflows, hyperpycnal deltas develop a greater subaqueous component at the price of a reduced subaerial component.

4. Applications and Implications

Having validated the analytical model with a range of experimental data, here we use this model as a tool to investigate comprehensively the effects of segmented bedrock slopes and Q/I ratio on the morphological features of Gilbert and hyperpycnal deltas. The subaerial features studied include shoreline $\lambda^{(2)}$ and topset length L_t , while the underwater feature studied is subaqueous volume V_f . Two types of phase diagrams are presented. To be useful, the conditions used here ($Q/I = 80 - 250$, $\theta_1 = 2^\circ - 10^\circ$, and $\theta_2 = 2^\circ - 5^\circ$) are comparable to those observed in many supply-limited bedrock rivers. The parameter values used (i.e.,

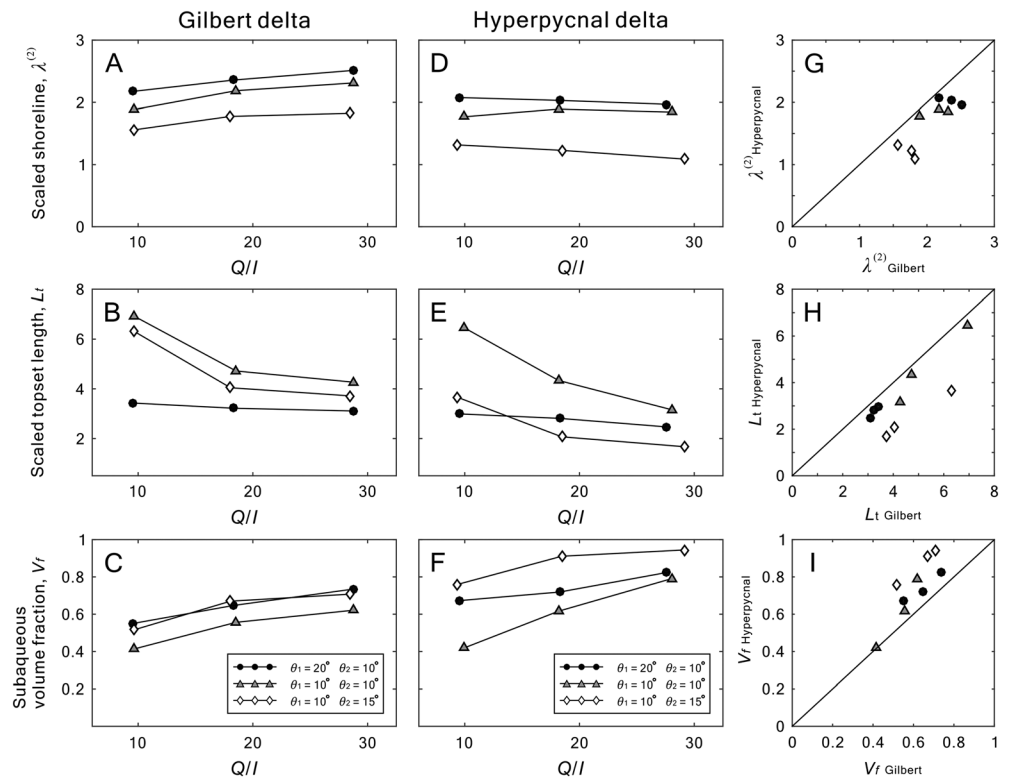


Figure 12. Variations of morphological features with Q/I ratio in different slope settings: (a and d) scaled shorelines $\lambda^{(2)}$; (b and e) scaled topset lengths L_t ; (c and f) subaqueous volume fractions V_f ; (g–i) comparison of $\lambda^{(2)}$, L_t , and V_f between Gilbert and hyperpycnal deltas.

diffusivities along the topset and foreset $\alpha_1 = 0.8$, $\alpha_2 = 0.8$) are well within the ranges determined from the experiments (see Table S1 for model parameters).

4.1. Phase Diagrams of Shoreline $\lambda^{(2)}$ Versus Subaqueous Volume V_f

Figure 13 shows the phase diagrams of shoreline $\lambda^{(2)}$ vs. subaqueous volume V_f as a function of the upstream and downstream slope angles (θ_1, θ_2) and Q/I ratio. In each panel, the upper half demonstrates the results associated with increasing θ_1 , while the lower half demonstrates the results associated with increasing θ_2 . In the upper half, θ_2 remains as 2° when θ_1 increases; in the lower half, θ_1 remains as 2° when θ_2 increases; the interface between them represents the single-slope setting $(\theta_1, \theta_2) = (2^\circ, 2^\circ)$. For each combination of (θ_1, θ_2) , the Q/I ratio varies from 80 to 250. For illustration purposes, in each panel we show six end members that correspond to the limiting values of $(\theta_1, \theta_2, Q/I)$. These include two groups of delta profiles: one along the small Q/I end, the other along the large Q/I end. Each group includes one delta profile at the steeper upstream end, one at the steeper downstream end, and one at the single-slope interface. Note that in the upper half of Figure 13b, all the data points corresponding to different $(\theta_1, Q/I)$ collapse to the single-slope interface. This arises because, as θ_2 is fixed as 2° , the longitudinal profiles of subaqueous delta components associated with different $(\theta_1, Q/I)$ are all similar triangles set by the angle of repose (see Figures 4d–4e), thus V_f would be held proportional to $\lambda^{(2)}$. In Figure 13b, different shapes and brightness of the colored symbols are used to differentiate the data points that correspond to different Q/I and θ_1 , respectively.

For hyperpycnal deltas (Figure 13a), the subaqueous volume V_f invariably increases with θ_1 , θ_2 , or Q/I . Migration of shoreline $\lambda^{(2)}$ accelerates with θ_1 but decelerates with θ_2 . The effect of Q/I ratio on shoreline migration is, however, nonmonotonic. For $\theta_1 > 2.5^\circ$ or $\theta_2 > 3^\circ$, shoreline migration decelerates with Q/I . For a limited range close to the single-slope setting, $2^\circ < \theta_1 < 2.5^\circ$ and $2^\circ < \theta_2 < 3^\circ$, shoreline migration

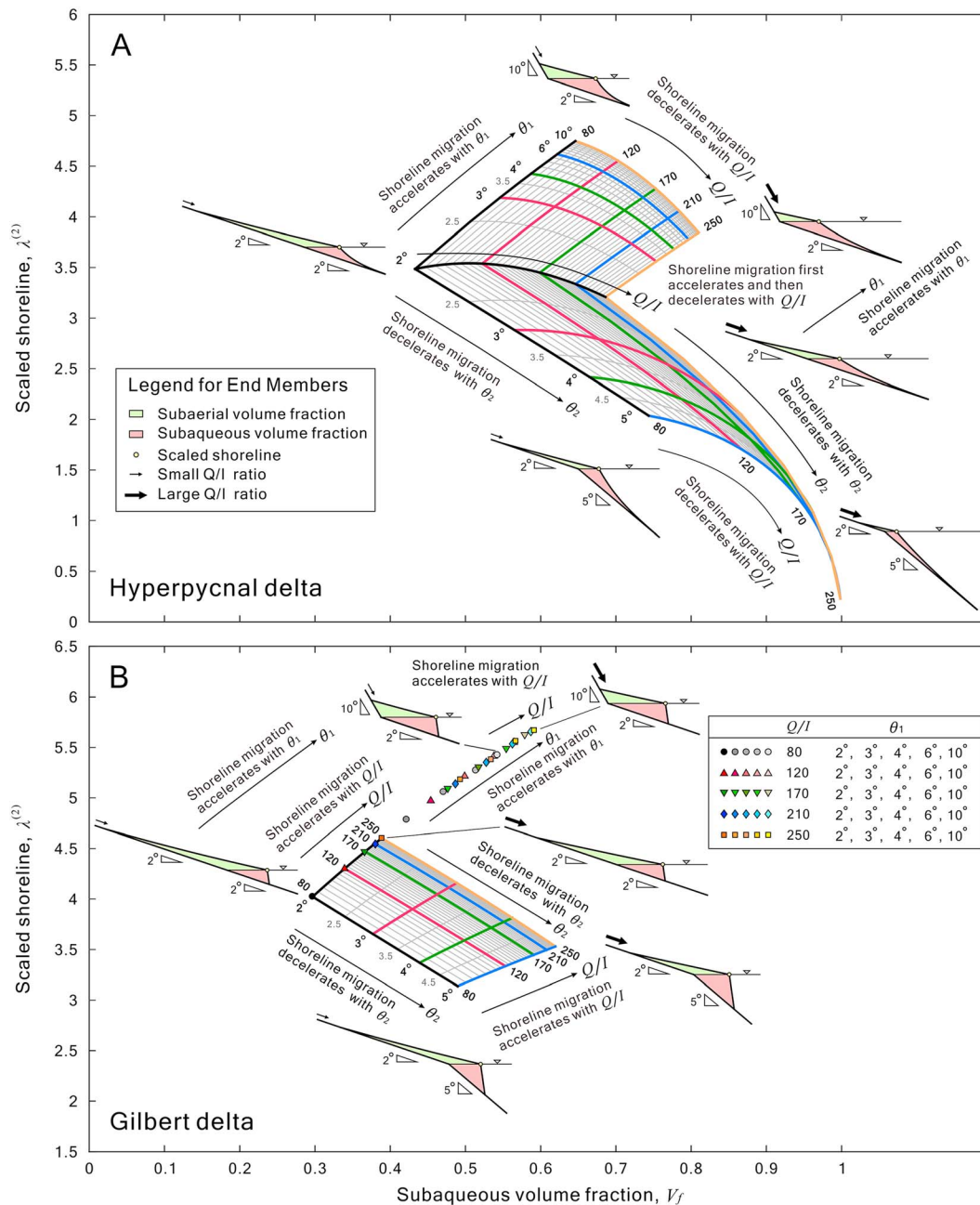


Figure 13. Phase diagrams of shoreline $\lambda^{(2)}$ versus subaqueous volume V_f as a function of the upstream and downstream slope angles (θ_1, θ_2) and Q/I . In the upper half of panels (a) and (b), θ_2 remains as 2° when θ_1 increases; in the lower half of each panel, θ_1 remains as 2° when θ_2 increases; the interface represents the single-slope setting (θ_1, θ_2) = ($2^\circ, 2^\circ$). For each combination of (θ_1, θ_2), Q/I varies from 80 to 250. Also shown are six end members with limiting values of (θ_1, θ_2) and Q/I . In panel (b), data corresponding to different ($\theta_1, Q/I$) collapse to the single-slope interface.

exhibits a first-accelerate-then-decelerate trend with Q/I , similar to those observed in Figures 11e and 12d. The presence of this nonmonotonic trend in the near-single-slope settings indicates that the effect of Q/I on shoreline migration emerges only when the two-slope effect is weak or absent. Away from the near-single-slope settings, the two-slope effect becomes dominant, thus suppressing the effect of Q/I . For Gilbert deltas (Figure 13b), however, monotonic trends are observed consistently. The subaqueous volume V_f increases with θ_1, θ_2 , or Q/I . Migration of shoreline $\lambda^{(2)}$ accelerates with θ_1 or Q/I but decelerates with θ_2 . These trends corroborate the results observed in Figures 12a and 12c.

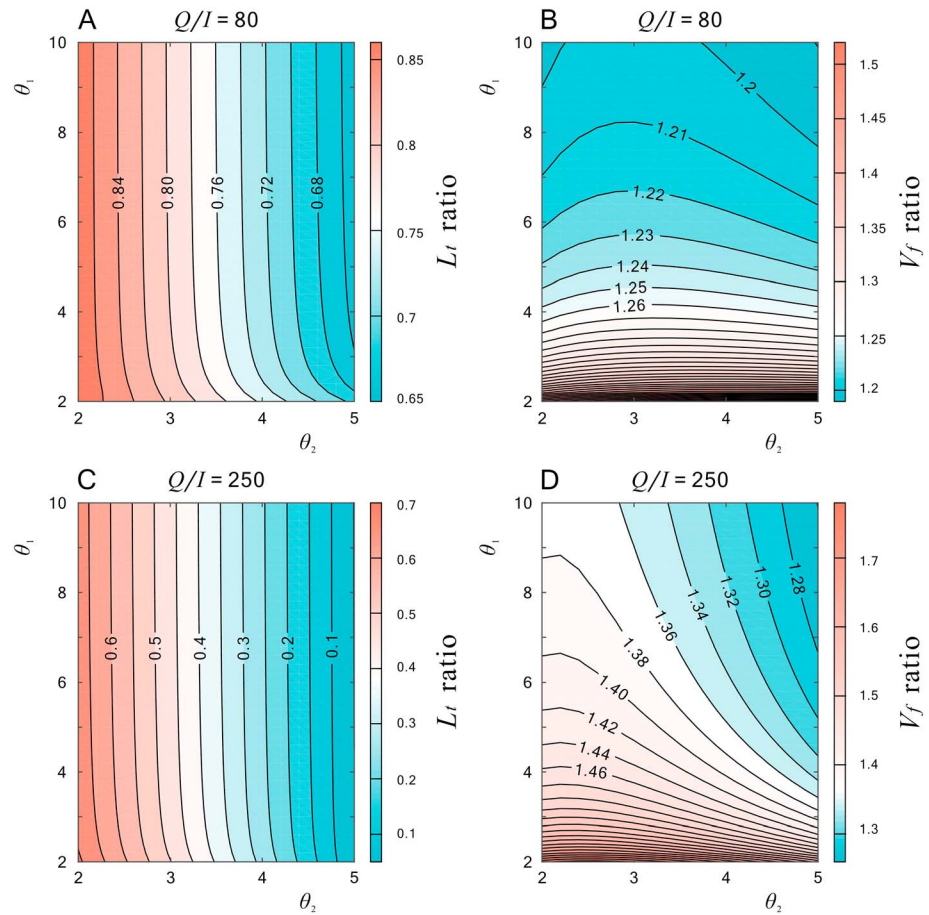


Figure 14. Phase diagrams of L_t ratio ($L_{t,\text{hyperpycnal}}/L_{t,\text{Gilbert}}$) and V_f ratio ($V_{f,\text{hyperpycnal}}/V_{f,\text{Gilbert}}$) as a function of the upstream and downstream slope angles (θ_1, θ_2): (a, b) for a lower $Q/I (=80)$; (c, d) for a higher $Q/I (=250)$.

4.2. Phase Diagrams of L_t Ratio and V_f Ratio

To elaborate on the results shown in Figures 12h and 12i, here we compare Gilbert and hyperpycnal deltas in terms of their topset lengths L_t and subaqueous volumes V_f . To this aim, we introduce two dimensionless parameters, termed L_t ratio and V_f ratio, which are defined as follows:

$$L_t \text{ ratio} = L_{t,\text{hyperpycnal}}/L_{t,\text{Gilbert}} \quad (4a)$$

$$V_f \text{ ratio} = V_{f,\text{hyperpycnal}}/V_{f,\text{Gilbert}} \quad (4b)$$

where subscript indicates the type of delta. Phase diagrams of L_t ratio and V_f ratio are depicted in Figure 14 over a range of θ_1 ($2^\circ - 10^\circ$) and θ_2 ($2^\circ - 5^\circ$), for a lower $Q/I (=80)$ and a higher $Q/I (=250)$. As can be seen, L_t ratios are invariably smaller than unity whereas V_f ratios are consistently greater than unity. These corroborate the results shown in Figures 12h and 12i; that is, Gilbert deltas have a larger subaerial component than their hyperpycnal counterparts, yet hyperpycnal deltas have a larger subaqueous component than their Gilbert-type counterparts.

With increasing Q/I , L_t ratios decrease from the range of values $\sim 0.6 - 0.9$ to $\sim 0.05 - 0.7$, while V_f ratios increase from the range of values $\sim 1.2 - 1.5$ to $\sim 1.3 - 1.8$. Variations of L_t ratio are dominated by the downstream slope (revealed by the nearly vertical isolines), while variations of V_f ratio are dominated by the upstream slope. Also, with increasing Q/I , the reduction of L_t ratio is more significant than the increase of V_f ratio. Collectively these results indicate that, as Q/I ratio increases, hyperpycnal deltas exhibit a relatively more drastic response in their subaerial component, which is dominated by variations of downstream basement slope.

4.3. Implications

The results presented herein carry practical implications for interpretation of the observed delta progradation into reservoir and for prediction of delta evolutions under future tectonic and climate scenarios or anthropogenic interventions. For example, the phase diagram shown in Figure 13a indicates that variation of upstream basement slope would reshape the delta profile such that the proportion of sediment deposits distributed in the subaqueous component would increase with θ_1 . This may explain why progradation of hyperpycnal delta into the Tarbela Reservoir was faster than expected even though the average sediment inflow was 64% lower than predicted (World Commission on Dams, 2000). Located in a tectonically active region, the upper Indus River is subjected to the increasing rate of tectonic uplift ranging between 4 and 10 mm/year (Korup et al., 2010; Leland et al., 1998), which has steepened the bedrock slope upstream of the Tarbela Reservoir over the last 20 Ma (Treloar et al., 1989). Continued uplift is further steepening the upstream segment, accelerating delta progradation and shoreline migration into the reservoir (Figure 13a), reducing the reservoir capacity and threatening the low-level facilities such as intake tunnels and outlets (Roca, 2012).

The multipurpose Tarbela Reservoir was designed to regulate seasonal flows for irrigation, power generation and flood control, with an ultimate aim of sustainable use. Reservoir operation may be optimized by minimizing water shortage and maximizing economic benefits while enhancing the sustainability through sediment evacuation (Khan & Tingsanchali, 2009; Roca, 2012; Tate & Farquharson, 2000). The optimal operating rules are typically determined via simulations of system performance under projected climate, land-use, and development scenarios. A critical ingredient is the storage versus elevation curve to be updated regularly by accounting for the accumulation of sediment (Dutta, 2016; Morris & Fan, 1998). In this regard, the phase diagram shown in Figures 13a may be useful for determining the distribution of subaqueous deposits and for predicting the morphological responses to alterations of natural and anthropogenic conditions.

Several factors affect the streamflow, sediment supply, and delta progradation into the reservoir. These include (1) tectonic uplift, (2) climate change, and (3) upstream reservoir facilities. The climatic impacts on streamflow and sediment supply reflect directly on Q/I . Given that ~90% of the annual water and sediment inflows are contributed by summer runoff from snow and glacier melt (Ali & de Boer, 2007; White, 2001), changes in temperature, snow precipitation, and snow/ice cover would impact the melting rate, streamflow, and sediment supply (Ali & de Boer, 2008). Simulation results under future climate scenarios indicate a doubling of summer runoff by 2050 (Tahir et al., 2011). In the snow- and glacier-fed subbasins of the upper Indus River, increasing the discharges by a factor of 2 would increase sediment supplies by a factor of 4.2 (Ali & de Boer, 2007), which in turn reduces the mean Q/I ratio by a factor of 2. Figure 13a indicates that a decrease in Q/I is associated with a reduction in subaqueous volume V_f , while an increase in upstream slope angle θ_1 (by tectonic uplift) is associated with an increase in V_f . Hence, there is a possibility that the uplift-induced increase in V_f could be counterbalanced by the climate-induced decrease in V_f . Phase diagrams of this kind can help predict future trends of reservoir sedimentation in response to the environmental changes.

Phase diagrams shown in Figure 14 can help predict the shift in delta morphology in response to the anthropic disturbances. Construction of the Basha Reservoir 315 km upstream from the Tarbela represents a new storage capacity and sediment trap that would alter the flow and sediment transport regimes. To be commissioned after 2020, the Basha Reservoir will operate in series with the Tarbela. The time series of inflow and water level in the Tarbela will change significantly, resulting in a 70% reduction of sediment inflow (Annandale et al., 2016; Roca, 2012). With much of the sediment load and summer runoff trapped in the Basha Reservoir, the Tarbela delta may transit from hyperpycnal to Gilbert-type in response to the changes in flow and sediment transport regimes (Lai & Capart, 2007). Figure 14 demonstrates the variation of V_f ratio over a range of (θ_1, θ_2) with an increase in Q/I . Considering the impact of future climate and operation scenarios on Q/I and steepening of upstream slope angle θ_1 by tectonic uplift, phase diagrams of this kind can help predict the trends of reservoir sedimentation where transition from hyperpycnal to Gilbert delta (or vice versa) takes place.

It should be noted that the phase diagrams provided in Figures 13 and 14 present the morphological features of delta under the given combinations of (θ_1, θ_2) and Q/I . These diagrams are meant to be used as a tool for predicting the trend of shift in delta morphologies for the projected slope settings or Q/I ratios. In case these

diagrams were used to predict the dynamic responses of deltas to changing tectonics or climate, the time-scales of these forcings must be taken into consideration. For example, for tectonics to be strong enough to change the bedrock slopes and steer the morphological shift, the deltaic timescale T_d must be greater than the tectonic timescale T_t , as suggested by Kim et al. (2010). Based on their approach, the tectonic timescale can be evaluated with $T_t = S_x/(\Delta\sigma_x/L_x)$, where S_x is the longitudinal bed slope, $\Delta\sigma_x$ is the uplift or subsidence rate over a longitudinal distance L_x . For the Tarbela delta shown in Figure 1b ($S_x = 5.8 \times 10^{-4}$, $\Delta\sigma_x = 4 - 10$ mm/year, and $L_x = 20$ km), the tectonic timescale would be $\sim 1,000 - 3,000$ years. This estimate of T_t is comparable to the tectonic timescale (2,200 years) estimated for the Ganges-Brahmaputra-Meghna delta (Reitz et al., 2015) and consistent with the finding that tectonics control the fluvial erosion rate over millennial to orogenic timescales (Koppes & Montgomery, 2009). It follows that, to be used to predict the morphodynamic response to changing tectonics, our results would apply for deltaic processes with $T_d >$ millennial timescale. Similarly, our results apply for deltaic processes with $T_d >$ centennial timescale when used to predict the morphodynamic response to lower-order climatic changes (Vandenberghe, 1995).

5. Conclusions

We investigate the morphodynamics of Gilbert and hyperpycnal deltas evolving over segmented two-slope bedrock channels. For both types of delta, the morphological responses to variations of the upstream or downstream basement slope are asymmetric. Steepening the upstream slope accelerates shoreline migration, steepening the downstream slope decelerates shoreline migration. In either case, the subaqueous delta volume is increased at the cost of reduced subaerial delta volume.

Through this study we seek to answer five research questions. First, hyperpycnal deltas, like Gilbert deltas, exhibit self-similar morphologies when evolving over segmented bedrock channels. Second, we demonstrate the underlying self-similarities in along-delta sediment flux and bed growth rate that come into play for attaining the self-similar delta morphologies. Third, under identical Q/I , Gilbert deltas exhibit faster shoreline migrations and longer topsets, while hyperpycnal deltas exhibit greater subaqueous volumes. These results suggest that, through enhanced sediment fluxes driven by dense underflows, hyperpycnal deltas develop a larger subaqueous component at the cost of a reduced subaerial component.

Fourth, Q/I ratio may be used to characterize the combined effect of flow and sediment supply. Increasing Q/I advances the entire delta, leading to a reduced topset and an enhanced subaqueous component. Fifth, the effects of Q/I on shoreline migration are inconsistent in different types of delta. For Gilbert deltas, shoreline migration accelerates with Q/I . For hyperpycnal deltas, the effect of Q/I is nonmonotonic. Within a limited range of slope combinations close to the single-slope setting, shoreline migration exhibits a first-accelerate-then-decelerate trend with increasing Q/I . Such trend in the near-single-slope range indicates that the effect of Q/I on shoreline migration emerges only if the two-slope effect is weak or absent. Away from this range, the two-slope effect becomes dominant, thus suppressing the effect of Q/I .

As applications, two types of phase diagram are presented that may be used to predict the trend of shift in delta morphologies under the projected slope settings or Q/I ratios. These results carry practical implications for interpretation of delta progradation into reservoir and prediction of delta evolutions under future tectonic and climate scenarios or anthropogenic interventions. A number of factors that are relevant to delta morphodynamics and stratigraphy, such as channel avulsion, base level change, density stratification, grain sorting, backwater, and wave/current dynamics are not incorporated and remain as prospective research tasks.

Notation

d_{50}	median grain size (L);
$f(\bar{x})$	dimensionless shape function (scaled delta profile) (-);
I	volumetric sediment influx per unit width (L^2/T);
\bar{j} , \bar{j}_0	scaled sediment flux ($=j/I$), and \bar{j} at $\bar{x}_s = 0$ (i.e., at aligned shorelines) (-);
L_t	scaled topset length (-);

Q	water inflow per unit width (L^2/T);
$s^{(1)}(t), s^{(2)}(t)$	evolving positions of bedrock-alluvial transition and shoreline (L);
t	time (T);
V_b, V_t	subaqueous and subaerial delta volume fractions (-);
(x, z)	horizontal and vertical coordinates (L);
(\bar{x}, \bar{z})	scaled horizontal and vertical coordinates (-);
\bar{x}_s	shifted \bar{x} coordinate aligning the shorelines at $\bar{x}_s = 0$ (-);
$z_0(x)$	elevation of bedrock basement (L);
α_1, α_2	dimensionless coefficients for diffusivities along the topset and foreset (-);
θ_1, θ_2	upstream and downstream basement slope angles (degree);
$\lambda^{(1)}, \lambda^{(2)}$	scaled positions of bedrock-alluvial transition and shoreline (-);
ρ_{in}, ρ_s	density of inflow, and density of sediment (ML^{-3});
ϕ	angle of repose (degree).

Acknowledgments

This study was supported by the Ministry of Science and Technology (MOST), Taiwan (grants to S. Y. J. L.: 107-2625-M-006-001 and 108-2119-M-006-007; F. C. W.: 106-2221-E-002-074-MY3 and 107-2221-E-002-029-MY3). We thank Yung-Tai Hsiao for the Gilbert delta experiments. We acknowledge Wonsuck Kim, three anonymous reviewers, and the Editors for feedbacks that helped improve the paper. The raw images, digitized profiles, and model parameters used herein are accessible from Zenodo repository (<http://doi.org/10.5281/zenodo.2410306>).

References

- Ahmed, K. B., & Sanchez, M. (2011). A study of the factors and processes involved in the sedimentation of Tarbela Reservoir, Pakistan. *Environment and Earth Science*, 62(5), 927–933. <https://doi.org/10.1007/s12665-010-0578-3>
- Ahmed, M. F., Rogers, J. D., & Ismail, E. H. (2018). Knickpoints along the upper Indus River, Pakistan: An exploratory survey of geomorphic processes. *Swiss Journal of Geosciences*, 111(1-2), 191–204. <https://doi.org/10.1007/s00015-017-0290-3>
- Ali, K. F., & de Boer, D. H. (2007). Spatial patterns and variation of suspended sediment yield in the upper Indus River basin, northern Pakistan. *Journal of Hydrology*, 334(3-4), 368–387. <https://doi.org/10.1016/j.jhydrol.2006.10.013>
- Ali, K. F., & de Boer, D. H. (2008). Factors controlling specific sediment yield in the upper Indus River basin, northern Pakistan. *Hydrological Processes*, 22(16), 3102–3114. <https://doi.org/10.1002/hyp.6896>
- Amos, K. J., Alexander, J., Horn, A., Pocock, G. D., & Fielding, C. R. (2004). Supply limited sediment transport in a high-discharge event of the tropical Burdekin River, North Queensland, Australia. *Sedimentology*, 51(1), 145–162. <https://doi.org/10.1111/j.1365-3091.2004.00616.x>
- Annandale, G. W., Morris, G. L., & Karki, P. (2016). *Extending the life of reservoirs*. Washington, DC: World Bank Publications, The World Bank Group.
- Capart, H., Bellal, M., & Young, D. L. (2007). Self-similar evolution of semi-infinite alluvial channels with moving boundaries. *Journal of Sedimentary Research*, 77(1), 13–22. <https://doi.org/10.2110/jsr.2007.009>
- Carraro, F., Vanzo, D., Caleffia, V., Valiani, A., & Siviglia, A. (2018). Mathematical study of linear morphodynamic acceleration and derivation of the MASSPEED approach. *Advances in Water Resources*, 117, 40–52. <https://doi.org/10.1016/j.advwatres.2018.05.002>
- Chavarrias, V., Blom, A., Orru, C., Martin-Vide, J. P., & Viparelli, E. (2018). A sand-gravel Gilbert delta subject to base level change. *Journal of Geophysical Research: Earth Surface*, 123, 1160–1179. <https://doi.org/10.1029/2017JF004428>
- Chikita, K. A., Smith, N. D., Yonemitsu, N., & Perez-Arluceas, M. (1996). Dynamics of sediment-laden underflows passing over a subaqueous sill: Glacier-fed Peyto Lake, Alberta, Canada. *Sedimentology*, 43(5), 865–875. <https://doi.org/10.1111/j.1365-3091.1996.tb01507.x>
- Dutta, S. (2016). Soil erosion, sediment yield and sedimentation of reservoir: A review. *Modeling Earth Systems and Environment*, 2(3), 123. <https://doi.org/10.1007/s40808-016-0182-y>
- Foreman, B. Z., Lai, S. Y. J., Komatsu, Y., & Paola, C. (2015). Braiding of submarine channels controlled by aspect ratio similar to rivers. *Nature Geoscience*, 8(9), 700–703. <https://doi.org/10.1038/ngeo2505>
- Gilbert, G. K. (1890). *Lake Bonneville, U.S. Geol. Surv. Monogr.* (Vol. 1, p. 438).
- Howard, A. D., & Kerby, G. (1983). Channel changes in badlands. *Geological Society of America Bulletin*, 94, 739–752.
- Khan, N. M., & Tingsanchali, T. (2009). Optimization and simulation of reservoir operation with sediment evacuation: A case study of the Tarbela Dam, Pakistan. *Hydrological Processes*, 23, 730–747.
- Kim, W., Sheets, B. A., & Paola, C. (2010). Steering of experimental channels by lateral basin tilting. *Basin Research*, 22, 286–301. <https://doi.org/10.1111/j.1365-2117.2009.00419.x>
- Kirby, E., & Whipple, K. X. (2012). Expression of active tectonics in erosional landscapes. *Journal of Structural Geology*, 44, 54–75.
- Koppes, M. N., & Montgomery, D. R. (2009). The relative efficacy of fluvial and glacial erosion over modern to orogenic timescales. *Nature Geoscience*, 2, 644–647.
- Korup, O., Montgomery, D. R., & Hewitt, K. (2010). Glacier and landslide feedbacks to topographic relief in the Himalayan syntaxes. *Proceedings of the National Academy of Sciences*, 107, 5317–5322.
- Kostic, S., Parker, G., & Marr, J. G. (2002). Role of turbidity currents in setting the foreset slope of clinoforms prograding into standing fresh water. *Journal of Sedimentary Research*, 72, 353–362.
- Lai, S. Y. J., & Capart, H. (2007). Two-diffusion description of hyperpycnal deltas. *Journal of Geophysical Research*, 112, F03005. <https://doi.org/10.1029/2006JF000617>
- Lai, S. Y. J., & Capart, H. (2009). Reservoir infill by hyperpycnal deltas over bedrock. *Geophysical Research Letters*, 36, L08402. <https://doi.org/10.1029/2008GL037139>
- Lai, S. Y. J., Gerber, T. P., & Amblas, D. (2016). An experimental approach to submarine canyon evolution. *Geophysical Research Letters*, 43, 2741–2747. <https://doi.org/10.1002/2015GL067376>
- Lai, S. Y. J., Hsiao, Y.-T., & Wu, F.-C. (2017). Asymmetric effects of subaerial and subaqueous basement slopes on self-similar morphology of prograding deltas. *Journal of Geophysical Research: Earth Surface*, 122, 2506–2526. <https://doi.org/10.1002/2017JF004244>
- Lai, S. Y. J., Hung, S. S. C., Foreman, B. Z., Limaye, A. B., Grimaud, J.-L., & Paola, C. (2017). Stream power controls the braiding intensity of submarine channels similarly to rivers. *Geophysical Research Letters*, 44, 5062–5070. <https://doi.org/10.1002/2017GL072964>

- Lanzoni, S., Siviglia, A., Frascati, A., & Seminara, G. (2006). Long waves in erodible channels and morphodynamic influence. *Water Resources Research*, 42, W06D17. <https://doi.org/10.1029/2006WR004916>
- Leland, J., Reid, M. R., Burbank, D. W., Finkel, R., & Caffee, M. (1998). Incision and differential bedrock uplift along the Indus River near Nanga Parbat, Pakistan Himalaya, from ^{10}Be and ^{26}Al exposure age dating of bedrock straths. *Earth and Planetary Science Letters*, 154, 93–107.
- Lorenzo-Trueba, J., Voller, V. R., Muto, T., Kim, W., Paola, C., & Swenson, J. B. (2009). A similarity solution for a dual moving boundary problem associated with a coastal-plain depositional system. *Journal of Fluid Mechanics*, 628, 427–443.
- Métivier, F., Lajeunesse, E., & Cacas, M.-C. (2005). Submarine canyons in the bathtub. *Journal of Sedimentary Research*, 75, 6–11.
- Montgomery, D. R., & Buffington, J. M. (1997). Channel-reach morphology in mountain drainage basins. *Geological Society of America Bulletin*, 109, 596–611.
- Morris, G. L., & Fan, J. (1998). *Reservoir Sedimentation Handbook*. New York: McGraw-Hill.
- Muto, T. (2001). Shoreline autoretreat substantiated in flume experiment. *Journal of Sedimentary Research*, 71, 246–254.
- Reitz, M. D., Pickering, J. L., Goodbred, S. L., Paola, C., Steckler, M. S., Seeber, L., & Akhter, S. H. (2015). Effects of tectonic deformation and sea level on river path selection: Theory and application to the Ganges-Brahmaputra-Meghna River Delta. *Journal of Geophysical Research: Earth Surface*, 120, 671–689. <https://doi.org/10.1002/2014JF003202>
- Roca, M. (2012). Tarbela Dam in Pakistan: Case study of reservoir sedimentation, In River Flow 2012, September 5-7, Costa Rica.
- Smith, D. G., & JoI, H. M. (1997). Radar structure of a Gilbert-type delta, Peyto Lake, Banff National Park, Canada. *Sedimentary Geology*, 113, 195–209.
- Sun, T., Paola, C., & Parker, G. (2002). Fluvial fan deltas: Linking channel processes with large-scale morphodynamics. *Water Resources Research*, 38(8), 1151. <https://doi.org/10.1029/2001WR000284>
- Tahir, A. A., Chevallier, P., Arnaud, Y., Neppel, L., & Ahmad, B. (2011). Modeling snowmelt-runoff under climate scenarios in the Hunza River basin, Karakoram Range, Northern Pakistan. *Journal of Hydrology*, 409, 104–117.
- Tate, E. L., & Farquharson, F. A. K. (2000). Simulating reservoir management under the threat of sedimentation: The case of Tarbela Dam on the River Indus. *Water Resources Management*, 14, 191–208.
- Treloar, P. J., Rex, D. C., Guise, P. G., Coward, M. P., Searle, M. P., Windley, B. F., et al. (1989). K-Ar and Ar-Ar geochronology of the Himalayan collision in NW Pakistan: Constraints on the timing of suturing, deformation, metamorphism and uplift. *Tectonics*, 8, 881–909.
- Uchida, T., Sakurai, W., Iuchi, T., Izumiyama, H., Borgatti, L., Marcato, G., & Pasutoc, A. (2018). Effects of episodic sediment supply on bedload transport rate in mountain rivers. Detecting debris flow activity using continuous monitoring. *Geomorphology*, 306, 198–209.
- Vandenbergh, J. (1995). Timescales, climate and river development. *Quaternary Science Reviews*, 14, 631–638.
- Voller, V. R., Swenson, J. B., & Paola, C. (2004). An analytical solution for a Stefan problem with variable latent heat. *International Journal of Heat and Mass Transfer*, 47, 5387–5390.
- Whipple, K. X., DiBiase, R. A., & Crosby, B. T. (2013). Bedrock rivers. In J. Shroder & E. Wohl (Eds.), *Treatise on geomorphology, Fluvial geomorphology* (Vol. 9, pp. 550–573). San Diego, CA: Academic Press. <https://doi.org/10.1016/B978-0-12-374739-6.00254-2>
- White, R. (2001). *Evacuation of Sediments from Reservoirs* (pp. 163–169). London: Thomas Telford Ltd.
- World Commission on Dams (2000). *Tarbela Dam and related aspects of the Indus River Basin Pakistan* (p. 212). Islamabad, Pakistan: Asianics Agro-Development International.
- Zgheib, N., Fedele, J. J., Hoyal, D. C. J. D., Perillo, M. M., & Balachandrar, S. (2018). Direct numerical simulation of transverse ripples: 2. Self-similarity, bedform coarsening, and effect of neighboring structures. *Journal of Geophysical Research: Earth Surface*, 123, 478–500. <https://doi.org/10.1002/2017JF004399>

References From the Supporting Information

- Swenson, J. B., Voller, V. R., Paola, C., Parker, G., & Marr, J. G. (2000). Fluvio-deltaic sedimentation: A generalized Stefan problem. *European Journal of Applied Mathematics*, 11, 433–452.
- Voller, V. R., Swenson, J. B., Kim, W., & Paola, C. (2006). A fixed grid method for moving boundary problems on the Earth's surface. *International Journal of Heat and Fluid Flow*, 16, 641–654.